

Two statistical procedures for mapping large-angle non-Gaussianity

W. Cardona

*Département de Physique Théorique, Université de Genève,
24 quai Ernest Ansermet, CH-1211 Genève 4, Switzerland*

A. Bernui

*Observatório Nacional
Rua General José Cristino 77
20921-400 Rio de Janeiro – RJ, Brazil*

M.J. Rebouças

*Centro Brasileiro de Pesquisas Físicas
Rua Dr. Xavier Sigaud 150
22290-180 Rio de Janeiro – RJ, Brazil*

(Dated: January 27, 2021)

A convincing detection of primordial non-Gaussianity in the cosmic background radiation (CMB) is essential to probe the physics of the early universe. Since a single statistical estimator can hardly be suitable to detect the various possible forms of non-Gaussianity, it is important to employ different statistical indicators to study non-Gaussianity of CMB. This has motivated the proposal of a number of statistical tools, including two large-angle indicators based on skewness and kurtosis of spherical caps of CMB sky-sphere. Although suitable to detect fairly large non-Gaussianity they are unable to detect non-Gaussianity within the Planck bounds, and exhibit power spectra with undesirable oscillation pattern. Simulated CMB maps are important tools to determine the strength, sensitivity and limitations of such non-Gaussian estimators. Here we use several thousands simulated CMB maps to examine interrelated problems regarding advances of these spherical patches procedures. We examine whether a change in the choice of the patches could enhance the sensitivity of the procedures well enough to detect large-angle non-Gaussianity within the Planck bounds. To this end, a new statistical procedure with non-overlapping cells is proposed and its capability is established. We also study whether this new procedure is capable to smooth out the undesirable oscillation pattern in the skewness and kurtosis power spectra of the spherical caps procedure. We show that the new procedure solves this problem, making clear this unexpected power spectra pattern does not have a physical origin, but rather presumably arises from the overlapping obtained with the spherical caps approach. Finally, we make a comparative analysis of this new statistical procedure with the spherical caps routine, determine their lower bounds for non-Gaussianity detection, and make apparent their relative strength and sensitivity.

PACS numbers: 98.80.Es, 98.70.Vc, 98.80.-k

I. INTRODUCTION

Recent cosmological observations are compatible with a nearly scale invariant spectrum of adiabatic perturbations [1, 2], which is predicted by a fair number of slow-roll single scalar inflationary models. In this way, there are many inflationary models that fit this power-spectrum feature. This fact calls for new statistical procedures to discriminate these models. A possible way to break this degeneracy among these models of the primordial universe is by studying deviation from Gaussianity of the cosmic microwave background (CMB) temperature fluctuations [3–10].

In single-field models of inflation, the amplitude of the local bispectrum can be written in terms of the slow-roll parameters and is undetectable ($|f_{\text{NL}}^{\text{local}}| \lesssim 10^{-6}$) [11, 12]. On the other hand, both multi-field inflationary models and other alternative scenarios predict typically a detectable level of local non-Gaussianity [13]. Therefore, a convincing detection of non-vanishing primordial non-

Gaussianity of local type ($f_{\text{NL}}^{\text{local}} \gg 1$) would rule out all the slow-roll single-field inflationary models and favour alternative models of the primordial universe [14] (see also, e.g., [5] and references therein).

In the study of deviation from Gaussianity of the CMB temperature fluctuations data, one is particularly interested in the component coming from the early stage of the universe. However, it is well known that there exist several contributions which do not have a primordial origin. Some non-primordial contributions come from un-subtracted diffuse foreground emission, unresolved point sources, possible systematic errors [15–20], and secondary anisotropies such as gravitational weak lensing and the Sunyaev–Zel’dovich effect [21–24]. Thus, the extraction of a possible primordial non-Gaussianity in CMB data is a challenging observational and statistical endeavor.

In this context, on the one hand we have that different statistical tools can potentially provide information about distinct features of non-Gaussianity [25–43]. On the other hand, one does not expect that a single

statistical estimator can be sensitive to all sorts of non-Gaussianity that may be present in observed CMB data. Thus, it is important to test CMB data for deviations from Gaussianity by using different statistical tools. This has motivated a great deal of effort that has recently gone into the search for non-Gaussianity in CMB maps by employing several statistical estimators and procedures [36–38, 44–66].

A simple way to possibly detect deviation from Gaussianity in the data of a given CMB map is by computing the skewness and kurtosis from the whole set of values of the temperature fluctuations. This procedure would furnish two dimensionless *global* numbers for describing the possible departures from non-Gaussianity of a CMB map. It is conceivable that in doing so one would lose local (directional) information concerning the non-Gaussianity of the CMB temperature fluctuations data. This has motivated the recent proposal of two large-angle non-Gaussianity statistical indicators [67, 68], whose chief idea is the following: starting from a given CMB temperature map one divides the CMB sphere \mathbb{S}^2 in j (say) spherical patches (subsets of CMB sky-sphere) whose union covers the whole CMB two-sphere. Then one calculates the skewness (S) and kurtosis (K) of each spherical region and patches them together to have two discrete functions $S(\theta, \phi)$ and $K(\theta, \phi)$ defined on \mathbb{S}^2 . These functions provide local measurements of the non-Gaussianity as a function of angular coordinates (θ, ϕ) . Their Mollweide projections are skewness and kurtosis maps (S -map and K -map). Motivated by the fact that simulated CMB maps with assigned type and amplitude of non-Gaussianity are important tools to study the sensitivity, limitations, and to determine the strength of non-Gaussian estimators, in a recent paper [69], by using overlapping spherical caps as the $j = 1, \dots, N_c$ regions to calculate S_j and K_j , it has been investigated whether and to what extent these non-Gaussian indicators have sensitivity to detect non-Gaussianity of local type, particularly with amplitude within the Wilkinson Microwave Anisotropy Probe (WMAP) bounds. A systematic study was made by employing this statistical procedure to generate maps of skewness and kurtosis from simulated maps equipped with non-Gaussianity of local type of various amplitudes. They have shown that S and K indicators, constructed through spherical overlapping caps, can be used to detect large-angle local-type non-Gaussianity only for reasonably large values of the non-linear parameter $f_{\text{NL}}^{\text{local}}$, typically $f_{\text{NL}}^{\text{local}} \gtrsim 500$. Thus, these indicators have not enough sensitivity to detect deviation from Gaussianity of local type with the non-linear parameter within the Planck bounds. Moreover, they have found that the power spectra of all S and K generated maps exhibit an unexpected *zig-zag* pattern (lower values for even ℓ modes versus higher values for neighboring odd modes), which does not seem to have a physical origin. These unexpected oscillations in the values of the even and odd modes in the power spectra could have been induced by overlapping of the spherical caps which con-

tain the temperature data used to construct the S and K maps.

Three possibly interrelated and pertinent questions arise naturally at this point. First, whether a change in the choice of the spherical patches (subsets of CMB sky-sphere) in the above practical procedure to construct the functions $S(\theta, \phi)$ and $K(\theta, \phi)$ would enhance the sensitivity of constructive routine well enough to detect non-Gaussianity of local type with $f_{\text{NL}}^{\text{local}}$ within the Planck bounds. Second, whether a suitable non-overlapping choice of spherical patches in the construction of $S(\theta, \phi)$ and $K(\theta, \phi)$ maps would be enough to smooth out the undesirable oscillation pattern in the power spectra of the S and K maps. Third, how could one compare the strength and weakness of the new spherical cells procedure with the caps routine of [67–69] in the attempts to detect large-angle ($\ell = 1, 2, 3, 4$) non-Gaussianity.

Our primary aim in this paper is to address these questions by using several thousands of simulated maps equipped with non-Gaussianity of local type of various amplitudes, extending therefore the results of Refs. [67–69] for a new improved version of non-Gaussianity statistical indicators S and K , where the spherical patches are a complete set of appropriately chosen equal area *non-overlapping large pixels* or *cells* of the CMB two-sphere. We examine the potentiality of the new version of the S and K statistical non-Gaussianity indicators and determine their efficacy and sensitivity to detect non-Gaussianity of local type whose amplitude are within and above the Planck limits. We show that the new non-Gaussianity indicators enhance sensitivity of the constructive routine to detect non-Gaussianity of local type for $f_{\text{NL}}^{\text{local}} \gtrsim 500$, but not for $f_{\text{NL}}^{\text{local}}$ within the Planck bounds. We also demonstrate that the new improved version of the indicators with non-overlapping patches do not give rise to oscillations in the values of the even and odd modes in the power spectra of S and K maps, solving this undesirable features of the previous indicators, and making clear that the oscillations do not have physical origin.

II. NON-GAUSSIANITY OF LOCAL TYPE AND SIMULATED MAPS

A. Primordial non-Gaussianity of Local Type

Quantum fluctuations in the very early universe seeded primordial gravitational curvature perturbations $\zeta(\mathbf{x}, t)$ which later generated the non-homogeneities in the distribution of matter we observe nowadays. In linear perturbation theory, the gauge invariant curvature perturbation ζ is related to the Bardeen’s potential $\Phi(\mathbf{x}, t)$ in the matter dominated era by $\zeta = (5/3)\Phi$ [70, 71]. On the other hand, on large scales the Sachs-Wolfe effect [72] relates CMB temperature fluctuations and gauge invariant

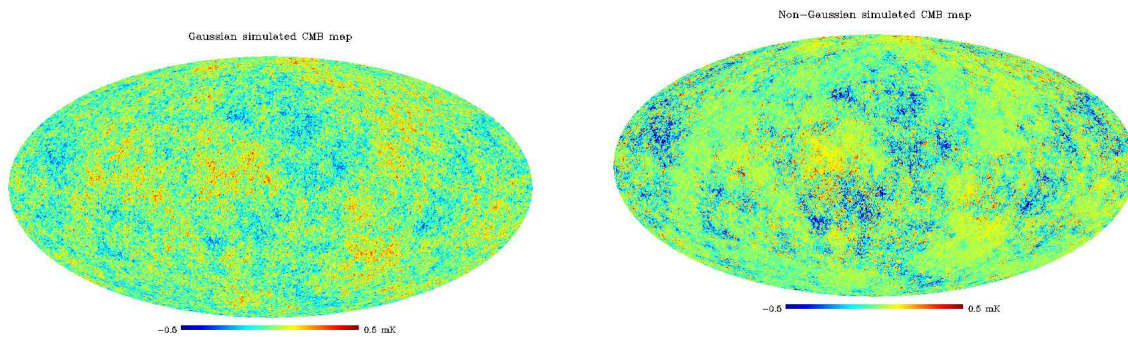


FIG. 1: Gaussian (left) and non-Gaussian (right) simulated CMB maps generated for $f_{\text{NL}}^{\text{local}} = 0$ and $f_{\text{NL}}^{\text{local}} = 5000$, respectively.

curvature perturbations through

$$\frac{\Delta T}{T} = -\frac{\zeta}{5} = -\frac{\Phi}{3}, \quad (1)$$

which allows to test inflationary models by comparing statistical properties of CMB data with those of ζ (and thus Φ) predicted by early universe models. Deviation from Gaussianity can be studied by using the three-point correlation function of the curvature perturbations $\Phi(\mathbf{x})$ or its Fourier transform $\Phi(\mathbf{k})$. The three-point correlation function in Fourier space or bispectrum is

$$\langle \Phi(\mathbf{k}_1)\Phi(\mathbf{k}_2)\Phi(\mathbf{k}_3) \rangle = \delta^{(3)}(\mathbf{k}_1 + \mathbf{k}_2 + \mathbf{k}_3) B_{\Phi}(k_1, k_2, k_3). \quad (2)$$

In the exam of primordial non-Gaussianity, the bispectrum of curvature perturbations is rewritten in the form

$$B_{\Phi}(k_1, k_2, k_3) = (2\pi)^3 f_{\text{NL}} F(k_1, k_2, k_3), \quad (3)$$

where f_{NL} is a dimensionless amplitude parameter which can be constrained by CMB observations, and $F(k_1, k_2, k_3)$ is a function of the magnitude of the wave numbers (k_1, k_2, k_3) called shape of the bispectrum. Single field models of inflation with standard kinetic terms and a Bunch-Davies vacuum predict a maximum for $F(k_1, k_2, k_3)$ in the so-called local configuration $k_1 \approx k_2 \gg k_3$ and amplitude $|f_{\text{NL}}^{\text{local}}| \lesssim 10^{-6}$. This is a remarkable result because a convincing detection of local non-Gaussianity would rule out all those single-field models [4, 5, 11, 12].

B. Simulated CMB Maps

Simulated CMB maps generated with a well-defined level and type of non-Gaussianity are essential tools to test the sensitivity and efficacy of non-Gaussian indicators. Simulated CMB maps endowed with local non-Gaussianity can be generated by noting that the Bardeen's potential Φ can reproduce the form of the bispectrum for the local configuration when parametrized in the form

$$\Phi(\mathbf{x}) = \Phi_{\text{L}}(\mathbf{x}) + f_{\text{NL}}^{\text{local}} [\Phi_{\text{L}}^2(\mathbf{x}) - \langle \Phi_{\text{L}}^2(\mathbf{x}) \rangle], \quad (4)$$

with $\Phi_{\text{L}}(\mathbf{x})$ being a Gaussian field with zero mean. This parametrization was used in Ref. [73] to build an algorithm which generates simulated CMB temperature and polarization maps endowed with local non-Gaussianity. In this algorithm a simulated map with a fixed level of non-Gaussianity $f_{\text{NL}}^{\text{local}}$ is defined by its spherical harmonic coefficients

$$a_{\ell m} = a_{\ell m}^{\text{L}} + f_{\text{NL}}^{\text{local}} \cdot a_{\ell m}^{\text{NL}}, \quad (5)$$

where $a_{\ell m}^{\text{L}}$ and $a_{\ell m}^{\text{NL}}$ are, respectively, the linear and non-linear spherical harmonic coefficients for the simulated CMB temperature map.¹

Figure 1 shows two examples of simulated CMB maps for $f_{\text{NL}}^{\text{local}} = 0$ (Gaussian) and $f_{\text{NL}}^{\text{local}} = 5000$ (non-Gaussian) with grid resolution $N_{\text{side}} = 512$, which we shall use throughout this paper.

III. NON-GAUSSIANITY WITH SPHERICAL CELLS PROCEDURE

A simple way for describing deviation from Gaussianity in CMB temperature fluctuations maps is by calculating the skewness $S = \mu_3/\sigma^3$, and the kurtosis $K = \mu_4/\sigma^4 - 3$ from the data, where μ_3 and μ_4 are the third and fourth central moments of the distribution of the temperature anisotropies, and σ is the variance. Considering that S and K vanish for a Gaussian distribution, two statistical estimators to measure large-angle deviation from Gaussianity in CMB maps were introduced in Ref. [67], from which a constructive general process can be formalized as follows. Let $\Omega_j \equiv \Omega(\theta_j, \phi_j) \in \mathbb{S}^2$ be the set of points of each spherical patch j for $j = 1, \dots, N$. One can define functions $S : \Omega_j \rightarrow \mathbb{R}$ and $K : \Omega_j \rightarrow \mathbb{R}$, that assign to

¹ These linear and non-linear coefficients are available at <http://planck.mpa-garching.mpg.de/cmb/fnl-simulations/>.

the j^{th} spherical patch two real numbers given by

$$S_j = \frac{1}{N_p \sigma_j^3} \sum_{i=1}^{N_p} (T_i - \bar{T})^3, \quad (6)$$

$$K_j = \frac{1}{N_p \sigma_j^4} \sum_{i=1}^{N_p} (T_i - \bar{T})^4 - 3, \quad (7)$$

where T_i is the temperature at the i^{th} pixel, \bar{T}_j is the CMB mean temperature of the j^{th} spherical patch Ω_j , N_p is the number of pixels in Ω_j , and $\sigma^2 = (1/N_p) \sum_{i=1}^{N_p} (T_i - \bar{T})^2$ is the standard deviation. Now, the set of all values S_j and K_j (calculated for all patches Ω_j 's) along with the angular coordinates of the center of the patch (θ_j, ϕ_j) are taken as measures of non-Gaussianity in the directions of the center of each spherical patch Ω_j . This constructive process defines two discrete functions $S = S(\theta, \phi)$ and $K = K(\theta, \phi)$ that give the deviation from Gaussianity on the sky-sphere \mathbb{S}^2 .

In this work, to define the skewness $S(\theta, \phi)$ and kurtosis $K(\theta, \phi)$ functions on \mathbb{S}^2 , instead of overlapping spherical caps of Refs. [67–69, 74] we take as spherical patches appropriately chosen equal area non-overlapping *large* pixels generated by the HEALPix partition of the CMB two-sphere [75] (see, e.g., Figure 2). Throughout this article, we call *spherical cell* or simply *cell* each one of these non-overlapping large pixels, and refer to the corresponding new routine as spherical cells (or simply cell) procedure. In brief, the spherical cells procedure can be formalized through the following steps:

1. For a given CMB (input) map with a determined grid resolution parameter N_{side} , divide the CMB sphere into 12 equal area *primary pixels* by using the HEALPix [75] partition of the sphere;²
2. Divide each one of the 12 primary pixels in $N_{\text{side}}'^2$ spherical cells, producing therefore $N_p' = 12 \times N_{\text{side}}'^2$ total number of cells (see, e.g., Figure 2);
3. Use equations (6) and (7) to calculate $S_j(\theta_j, \phi_j)$ and $K_j(\theta_j, \phi_j)$ for each $j = 1, \dots, N_p'$ cells;
4. Patch together S_j and K_j to define the discrete functions $S(\theta, \phi)$ and $K(\theta, \phi)$ on \mathbb{S}^2 , whose Mollweide projection are, respectively, S and K maps. These maps give a directional (geographical) distribution of values of skewness and kurtosis calculated from a given CMB input map.

As a practical application of this statistical procedure, figures 2 and 3 show, respectively, S and K maps with 48 spherical cells ($N_{\text{side}}' = 2$) computed from CMB input

maps depicted in Fig. 1. As expected, S and K maps for Gaussian ($f_{\text{NL}}^{\text{local}} = 0$) CMB simulated maps present a roughly uniform low values (close colors) distribution for the skewness and kurtosis, whereas those maps calculated from the non-Gaussian CMB simulated input maps with $f_{\text{NL}}^{\text{local}} = 5000$ present inhomogeneous higher values distribution for the skewness and kurtosis.

Now, since the functions $S = S(\theta, \phi)$ and $K = K(\theta, \phi)$ are discrete functions defined on \mathbb{S}^2 they can be expanded into their spherical harmonics, and one can calculate their angular power spectra. Thus, for example, for $K(\theta, \phi)$ one has

$$K(\theta, \phi) = \sum_{\ell=0}^{\infty} \sum_{m=-\ell}^{\ell} b_{\ell m} Y_{\ell m}(\theta, \phi), \quad (8)$$

and the corresponding angular power spectrum

$$K_{\ell} = \frac{1}{2\ell + 1} \sum_m |b_{\ell m}|^2. \quad (9)$$

Clearly, one can similarly expand the skewness function $S(\theta, \phi)$ and calculate its angular power spectrum S_{ℓ} . In the next section we shall use the power spectra S_{ℓ} and K_{ℓ} to assess the departure from Gaussianity, i.e. to calculate the statistical significance of such a deviation by comparison with the corresponding power spectra calculated from input Gaussian maps ($f_{\text{NL}}^{\text{local}} = 0$), and determine their suitability of the cellular procedure to detect non-Gaussianity.

IV. ANALYSES AND RESULTS

In this section we report the results of our analyses of non-Gaussianity carried out by using the $S(\theta, \phi)$ and $K(\theta, \phi)$ functions and associated S and K maps, constructed through the spherical cells procedure, described in Sec. III, along with several thousands of simulated CMB maps equipped with non-Gaussianity of local type.

First, we note that in order to have a reference for comparing non-Gaussianity, we have generated 1000 S and 1000 K maps from 1000 CMB Gaussian ($f_{\text{NL}}^{\text{local}} = 0$) simulated maps, and have computed their angular power spectra $S_{\ell}^{\mathbf{i}}$ and $K_{\ell}^{\mathbf{i}}$ ($\mathbf{i} = 1, \dots, 1000$ is an enumeration index) to have the mean angular power spectra $S_{\ell} = (1/1000) \sum_{\mathbf{i}=1}^{1000} S_{\ell}^{\mathbf{i}}$ and similarly the mean spectra K_{ℓ} . A similar procedure has been used several times to calculate the mean angular power spectra from 1000 S maps, and of 1000 K maps computed from 1000 CMB non-Gaussian maps with different $f_{\text{NL}}^{\text{local}}$ in each instance.

We have measured the statistical significance of the deviations from Gaussianity through a χ^2 test to find out the departure from goodness of the fit between mean power spectra calculated from Gaussian maps ($f_{\text{NL}}^{\text{local}} = 0$), S_{ℓ}^G and K_{ℓ}^G , and mean angular power spectra computed from non-Gaussian ($f_{\text{NL}}^{\text{local}} \neq 0$) maps, S_{ℓ}^{NG} and K_{ℓ}^{NG} . In other words, we have used χ^2 test along with the power spectra

² With the HEALPix partition of the sphere, the total number of pixels for the map equals $N_p^{\text{total}} = 12 \times N_{\text{side}}^2$.

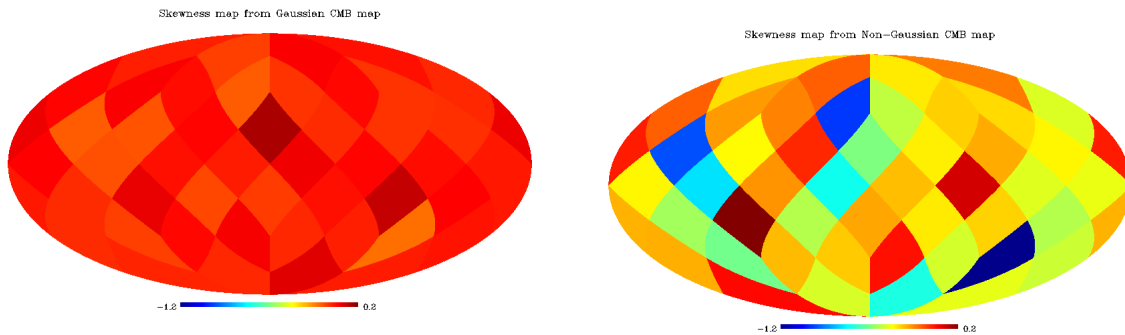


FIG. 2: Skewness maps calculated by using the spherical cells procedure with 48 cells along with simulated CMB input maps depicted in Fig. 1, whose amplitude of non-Gaussianity are $f_{\text{NL}}^{\text{local}} = 0$ (left panel) and $f_{\text{NL}}^{\text{local}} = 5000$ (right panel), respectively. Each colored large pixel (patch) is called a spherical cell.

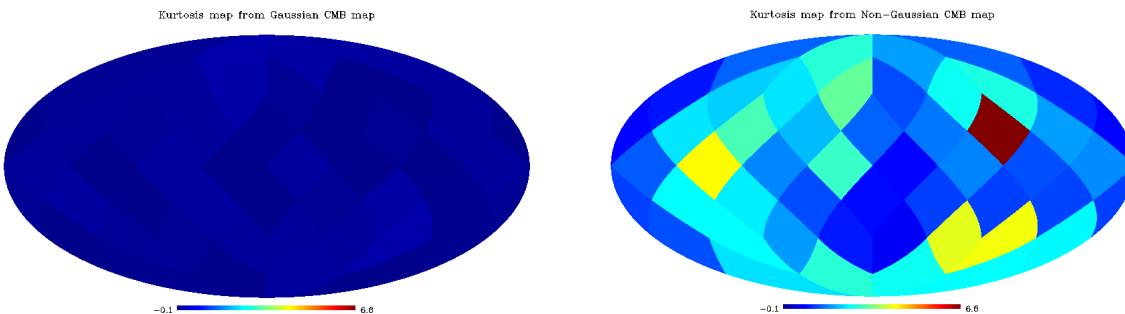


FIG. 3: Kurtosis maps generated through the spherical cells routine with 48 cells along with simulated CMB input maps depicted in Fig. 1, for which $f_{\text{NL}}^{\text{local}} = 0$ (left panel) and $f_{\text{NL}}^{\text{local}} = 5000$ (right panel), respectively.

to assess the significance of the deviation from Gaussianity.

In this way, for the indicator S (similar expression holds for K) one has

$$\chi_{S_\ell}^2 = \frac{1}{n-1} \sum_{\ell=1}^n \frac{(S_\ell^{\text{NG}} - S_\ell^{\text{G}})^2}{(\sigma_\ell^{\text{G}})^2}, \quad (10)$$

where S_ℓ^{G} and S_ℓ^{NG} are the mean values for each ℓ mode, $(\sigma_\ell^{\text{G}})^2$ is the variance calculate from Gaussian maps, and $n = 4$ is the highest multipole permitted for the grid resolution of 48 cells we have employed.

Clearly the greater is this value the smaller is the associated χ^2 probability, i.e. the smaller is the probability that the mean multipoles values S_ℓ and K_ℓ calculated from a given non-Gaussianity map ($f_{\text{NL}}^{\text{local}} \neq 0$) and the mean multipole values obtained from ($f_{\text{NL}}^{\text{local}} = 0$) agree. We have employed this procedure to the analyses whose results we shall report in the following.

In order to choose the most suitable number of cells in the procedure, we have examined how the behavior of S and K indicators is affected by the number of cells used to construct $S(\theta, \phi)$ and $K(\theta, \phi)$ functions and associated maps. To this end, we have used non-Gaussian simulated CMB maps with local non-Gaussian amplitude $f_{\text{NL}}^{\text{local}}$ in

$f_{\text{NL}}^{\text{local}}$	48 cells		192 cells	
	$\chi_{S_\ell}^2$	$\chi_{K_\ell}^2$	$\chi_{S_\ell}^2$	$\chi_{K_\ell}^2$
20	1.01×10^{-5}	2.41×10^{-5}	2.57×10^{-6}	3.46×10^{-6}
56	1.04×10^{-3}	9.43×10^{-4}	2.42×10^{-4}	1.53×10^{-4}
100	9.62×10^{-3}	6.63×10^{-3}	2.22×10^{-3}	1.13×10^{-3}
400	3.14×10^{-1}	1.80×10^{-1}	5.63×10^{-1}	2.60×10^{-1}
500	5.88	4.05	1.38	7.04×10^{-1}
1000	9.19×10	1.74×10^2	2.33×10	4.04×10
3000	3.02×10^3	2.67×10^9	1.13×10^3	1.56×10^9
5000	7.76×10^3	4.95×10^9	4.10×10^3	2.02×10^9

TABLE I: χ^2 values calculated from the mean power spectra S_ℓ and K_ℓ of S and K maps computed from simulated temperature maps for 8 values of $f_{\text{NL}}^{\text{local}}$ including the Planck limits. The spherical cells procedure with 48 and 192 cells was employed to generate the S and K maps

the limits of the interval found by Planck experiment,³ as well as several other values for the amplitude of local non-

³ We stress that given the resolution of the simulated maps used in this work, we have taken the $f_{\text{NL}}^{\text{local}}$ limits for $\ell_{\text{max}} = 500$ of the SMICA cleaned maps as reported in the table 16 of Ref. [76], that is, 38 ± 18 .

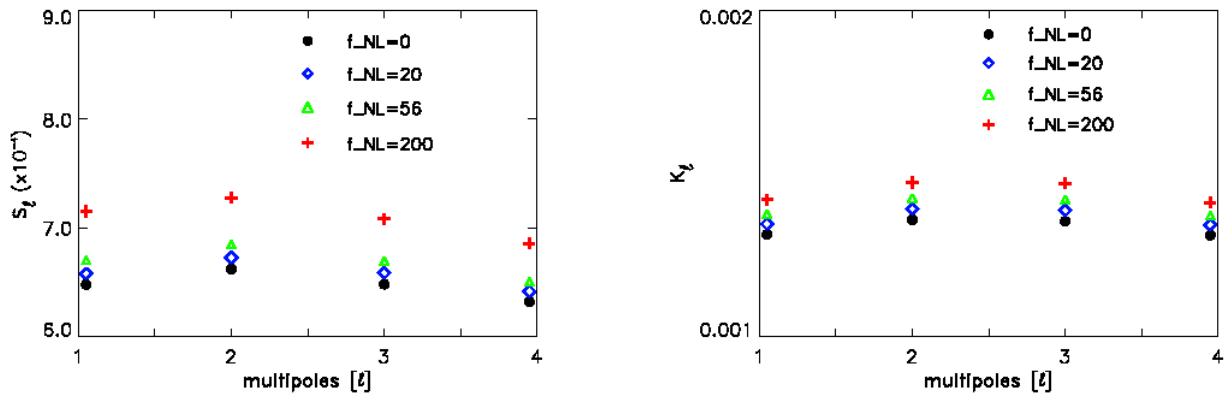


FIG. 4: Low ℓ angular power spectra S_ℓ (left panel) and K_ℓ (right panel) of S and K maps generated from simulated CMB input maps equipped with non-Gaussianity of local type whose values of the amplitude parameter are $f_{\text{NL}}^{\text{local}} = 20, 56$ (Planck limits) as well as $f_{\text{NL}}^{\text{local}} = 0$ (Gaussian) and $f_{\text{NL}}^{\text{local}} = 200$ (illustrative value).

Gaussianity (see Table I). For each value of $f_{\text{NL}}^{\text{local}}$ we have generated 1000 simulated CMB input maps, from which we have calculated 1000 S and 1000 K maps by using 48 and 192 cells and the associated power spectra S_ℓ^i and K_ℓ^i to have the mean power spectra S_ℓ^{NG} and K_ℓ^{NG} , which were used to finally compute the $\chi^2_{S_\ell}$ and $\chi^2_{K_\ell}$ collected together in Table I.⁴ The results of the χ^2 analysis in this table show that the spherical cells procedure, with both 48 and 192 cells, do not have sufficient sensitivity to detect deviation from non-Gaussianity for the values of the non-Gaussian parameter within the Planck bounds $20 \leq f_{\text{NL}}^{\text{local}} \leq 56$. Indeed, for simulated maps whose amplitude parameter $f_{\text{NL}}^{\text{local}}$ are equal to the Planck bounds one has a negligible value of χ^2 , which makes apparent that there is no significant overall departure of the mean power spectra S_ℓ^{NG} and K_ℓ^{NG} and the associated power spectra obtained from Gaussian maps (χ^2 -probability is virtually equal to 1). In Fig. 4 we illustrate this result by showing the nearly overlapping of the symbols corresponding to $f_{\text{NL}}^{\text{local}} = 0, 20, 56$. For visual comparison, in Fig. 4 we also present the result for $f_{\text{NL}}^{\text{local}} = 200$.

To the extent that the average S_ℓ and K_ℓ obtained from simulated CMB maps endowed with $f_{\text{NL}}^{\text{local}} = 500$ are within 95% average values of S_ℓ and K_ℓ for $f_{\text{NL}}^{\text{local}} = 0$, Table I shows that spherical cells procedures are not suitable to detect primordial non-Gaussianity of local type in CMB maps smaller than $f_{\text{NL}}^{\text{local}} = 500$. Table I also shows that for non-Gaussianity amplitude $f_{\text{NL}}^{\text{local}} \geq 500$ the spherical cells procedure with 48 cells is more suitable than with 192 cells, inasmuch as it detects values for

χ^2 greater than the values obtained for 192 cells. This favors the use of 48 cells in the comparative analysis of the spherical cells and caps procedures, which we shall discuss in what follows.

$f_{\text{NL}}^{\text{local}}$	48 cells		3072 Caps	
	$\chi^2_{S_\ell}$	$\chi^2_{K_\ell}$	$\chi^2_{S_\ell}$	$\chi^2_{K_\ell}$
20	1.01×10^{-9}	2.41×10^{-9}	8.33×10^{-3}	5.07×10^{-3}
56	1.04×10^{-3}	9.43×10^{-4}	8.58×10^{-3}	5.3×10^{-3}
500	5.88	4.05	4.5×10^{-4}	3.58×10^{-3}
1000	9.19×10	1.74×10^2	6.05×10^{-3}	9.79×10^{-2}
3000	3.02×10^3	2.67×10^9	2.16×10^{-1}	2.77×10
5000	7.76×10^3	4.95×10^9	5.64×10^{-1}	1.53×10^2

TABLE II: χ^2 values calculated from the mean power spectra S_ℓ and K_ℓ of S and K maps computed from simulated temperature maps for 6 values of $f_{\text{NL}}^{\text{local}}$ including the Planck limits. The spherical cells procedure with 48 and the spherical caps method with 3072 caps were used for comparison of these two approaches.

Having determined the most appropriated number of cells in the cellular procedure, we have made an analysis to compare the spherical cells strategy with the spherical cap procedure employed in Refs. [67–69] (see also related paper [77]). We have also examined whether the unexpected *zig-zag* power spectra patterns of S and K maps, obtained through the spherical caps procedure, is solved by the cells approach as it is preliminary indicated by Fig. 4. Table II along with Fig. 5 contain the results of our calculations carried out by using a total of 24000 S and K simulated maps. This table shows that both versions of the procedures can be used to detect *large-angle* ($\ell = 1, 2, 3, 4$) local-type non-Gaussianity only for fairly large values of the non-linear parameter $f_{\text{NL}}^{\text{local}}$, namely $f_{\text{NL}}^{\text{local}} \geq 500$ for the cells procedure, and $f_{\text{NL}}^{\text{local}} \geq 3000$ for the spherical caps (here through the K indicator). Thus, to the extent that for all $f_{\text{NL}}^{\text{local}} \geq 500$, χ^2 test gives

⁴ To construct the Table I we have generated a total of 45000, of which 9000 were simulated temperature CMB (input) maps for different $f_{\text{NL}}^{\text{local}}$ including the Gaussian maps, and 18000 S -maps and 18000 K -maps computed in each case by using both 48 and 192 cells.

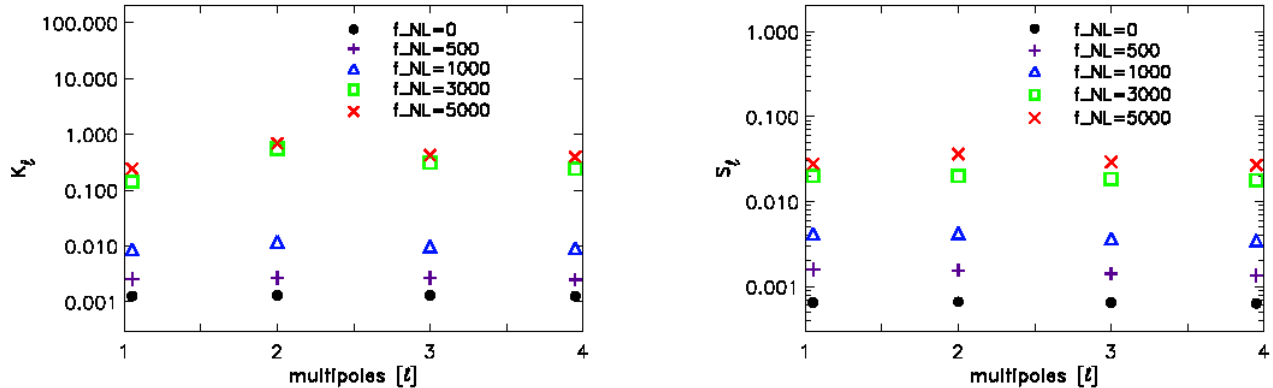


FIG. 5: Low ℓ angular power spectra, K_ℓ and S_ℓ , of K maps (left panel) and of S maps (right panel), respectively, calculated from both Gaussian and non-Gaussian ($0 \leq f_{\text{NL}}^{\text{local}} \leq 5000$) simulated CMB maps by using the spherical cells method with 48 spherical cells.

greater values for the cells procedure than for the caps approach, Table II shows that the spherical cells procedure is more suitable to detect large-angle ($\ell = 1, 2, 3, 4$) local-type non-Gaussianity than the spherical caps procedure used in Refs. [67–69].

The panels of Fig 5 preset the low ℓ mean power spectra of the skewness S_ℓ (left panel) and kurtosis K_ℓ (right panel), calculated from 1000 Gaussian ($f_{\text{NL}}^{\text{local}} = 0$) maps, and 4000 non-Gaussian input simulated CMB maps equipped with Non-Gaussianity of the local type for which $f_{\text{NL}}^{\text{local}} = 500, 1000, 3000, 5000$. These panels reassert the results preliminary detected in Fig. 4, namely they show that the oscillations in the values of the even and odd modes in the power spectra S_ℓ and K_ℓ that occur in the overlapping spherical caps procedure (see, for example, Fig. 6 in Ref. [67], Fig. 3 in Ref. [68] and Fig. 4 of Ref. [69]) do not come out in the Fig 5, obtained through the spherical cells approach, making clear that this unexpected power spectra pattern does not have a physical origin, but rather arises presumably from the overlapping of the spherical caps.

V. CONCLUDING REMARKS

The physics of the very early universe can be probed by measuring the statistical properties of the temperature fluctuations in the CMB data. Since different classes of such models predict different types and levels of non-Gaussianity for CMB anisotropies, by studying primordial non-Gaussianity of CMB data one could discriminate or even rule out either inflationary models or alternative scenarios to the inflationary paradigm. In this context, it is important to test CMB data for deviations from Gaussianity by using different statistical tools to assess and constrain the amount of any non-Gaussian signals in the data, and extract information about their potential

origins. Furthermore, one does not expect that a single statistical estimator to be sensitive to all possible forms of non-Gaussianity, which could be present in CMB data.

Recently, two large-angle non-Gaussianity indicators S and K based on skewness and kurtosis of spherical caps of CMB sky-sphere have been proposed and used to study large-angle deviation from Gaussianity in masked frequency bands and foreground-reduced full sky CMB maps [67, 68]. Even though these indicators can be used to detect non-Gaussianity signals in CMB data, it has been shown [69] by using simulated maps that they are not suitable to discover local non-Gaussianity for the amplitude parameter $f_{\text{NL}}^{\text{local}}$ within the current observational bounds. Moreover, they have found that the power spectra of S and K maps exhibit an unexpected oscillation in the values of the even and odd modes in the S_ℓ and K_ℓ mean spectra, which could have been induced by overlapping of the patches in the spherical cap procedure.

In this paper we have addressed three interrelated questions regarding advances of the spherical patches procedures for the detection of large-angle non-Gaussianity. First, we have examined whether a change in the choice of the patches would enhance the sensitivity of a new constructive procedure well enough to detect large-angle non-Gaussianity of local type with $f_{\text{NL}}^{\text{local}}$ within the Planck bounds. Second, we have studied whether this new procedure with suitable non-overlapping choice of spherical patches would be capable to smooth out the undesirable oscillation pattern in the power spectra of the associated skewness and kurtosis maps. Third, we have additionally made a comparative analysis of the new spherical cells procedure with the caps routine of [67–69] to find out their relative strength and weakness in the study of large-angle ($\ell = 1, 2, 3, 4$) non-Gaussianity.

To this end, we have employed the two procedures along with 9000 simulated CMB temperature maps equipped with non-Gaussianity of local type with various

amplitudes. From these simulated maps, which include the Gaussian ones with $f_{\text{NL}}^{\text{local}} = 0$, we have generated 24 000 S -maps and 24 000 K -maps (for 48 and 192 cells and 3 072 caps), calculated the low ℓ mean power spectra S_ℓ and K_ℓ , made a study of the sensitivity and strength, and determined the limitations of non-Gaussian estimators S and K . The results of our analyses are summarized in Tables I and II together with Fig. 2 to Fig. 5

The negligible value of χ^2 analysis collected together in Table I shows, on the one hand, that the spherical cells new procedure, with both 48 and 192 cells, do not have sufficient sensitivity to detect local non-Gaussianity for the amplitude parameter within the Planck bounds $20 \leq f_{\text{NL}}^{\text{local}} \leq 56$. Figure 4 complements this result by showing the nearly overlapping of the symbols for $f_{\text{NL}}^{\text{local}} = 0, 20, 56$. On the other hand, Table I also makes clear that for non-Gaussianity amplitude $f_{\text{NL}}^{\text{local}} \geq 500$ the spherical cells procedure with 48 cells is more suitable to detect local non-Gaussianity than with 192 cells.

Table II shows that both versions of the procedures can be used to detect large-angle ($\ell = 1, 2, 3, 4$) local-type non-Gaussianity for reasonably large values of the amplitude parameter $f_{\text{NL}}^{\text{local}}$, namely $f_{\text{NL}}^{\text{local}} \geq 500$ for the cells procedure, and $f_{\text{NL}}^{\text{local}} \geq 3000$ for the spherical caps. Thus, Table II shows that the spherical cells procedure is more suitable to detect large-angle local-

type non-Gaussianity than the spherical caps procedure of Refs. [67–69].

Finally, the panels of Fig 4 and Fig. 5 show that the oscillations in the values of the even and odd modes in the power spectra S_ℓ and K_ℓ of the overlapping spherical caps procedure do not come about in these figures obtained through the spherical cells procedures. This makes clear that the power spectra unexpected patterns of the caps procedure do not have a physical origin, but rather arises presumably from the overlapping of the spherical caps.

Acknowledgments

We would like to thank Martin Kunz for helpful discussions, important comments and suggestions. We are grateful to A.F.F. Teixeira for reading the manuscript and indicating some omissions and typos. M.J. Rebouças acknowledges the support of FAPERJ under a CNE E-26/102.328/2013 grant. A. Bernui, and M.J. Rebouças thank CNPq for the grants under which this work was carried out. W. Cardona is supported by COLCIENCIAS and acknowledges financial support by CNPq in the early stage of this work. Some of the results in this paper were derived using the HEALPix package[75].

-
- [1] Planck Collaboration: P.A.R. Ade, et al., arXiv:1303.5076
- [2] Planck Collaboration: P.A.R. Ade, et al., arXiv:1303.5082
- [3] N. Bartolo, E. Komatsu, S. Matarrese, A. Riotto, Phys. Rept. **402**, 103 (2004)
- [4] E. Komatsu, et al., arXiv:0902.4759
- [5] E. Komatsu, Class. Quant. Grav. **27**, 124010 (2010)
- [6] X. Chen., Adv. in Astron., 638979 (2010)
- [7] M. Kawasaki, K. Nakayama, F. Takahashi, JCAP **01**, 026 (2009)
- [8] M. Kawasaki, K. Nakayama, T. Sekiguchi, T. Suyama, F. Takahashi, JCAP **01**, 04 (2009)
- [9] D. Pogosyan, C. Pichon, C. Gay, Phys. Rev. D **84**, 083510 (2011)
- [10] M. Sasaki, D. Wands, Class. Quant. Grav. **27**, 120301 (2010)
- [11] J. Maldacena, JHEP **05**, 013 (2003)
- [12] V. Acquaviva, N. Bartolo, S. Matarrese, A. Riotto, Nucl. Phys. B **667**, 119 (2003)
- [13] K. Koyama, S. Mizuno, F. Vernizzi, D. Wands, JCAP **11**, 024 (2007); E.I. Buchbinder, J. Khoury, B.A. Ovrut, Phys. Rev. Lett. **100**, 171302 (2008); J.L. Lehners, P.J. Steinhardt, Phys. Rev. D **77**, 063533 (2008); J.L. Lehners, Phys. Rept. **465**, 223 (2008); Y.-F. Cai, W. Xue, R. Brandenberger, X. Zhang, JCAP **05**, 011 (2009)
- [14] P. Creminelli, M. Zaldarriaga, JCAP **10**, 006 (2004)
- [15] L.-Y. Chiang, P.D. Naselsky, O.V. Verkhodanov, M.J. Way, Astrophys. J. Suppl. Ser. **590**, L65 (2003)
- [16] P.D. Naselsky, O.V. Verkhodanov, L.-Y. Chiang, I.D. Novikov, Int. J. mod. Phys. D **14**, 1273 (2005)
- [17] J. Delabrouille, et al., arXiv: 0807.0773
- [18] P.K. Aluri, P.K. Rath, P. Jain, arXiv:1202.2678
- [19] M. Cruz, P. Vielva, E. Martínez-González, R.B. Barreiro, Mon. Not. Roy. Astron. Soc. **412**, 2383 (2011)
- [20] R. Saha, Astrophys. J. **739**, L56 (2011)
- [21] N. Aghanim, S. Majumdar, J. Silk, Rep. Prog. Phys. **71**, 066902 (2008)
- [22] D. Munshi, A. Heavens, A. Cooray, P. Valageas, Mon. Not. Roy. Astron. Soc. **414**, 3173 (2011)
- [23] F. Pace, et al., Mon. Not. Roy. Astron. Soc. **411**, 595 (2011)
- [24] C.P. Novaes, C.A. Wuensche, Astron. Astrophys. **545**, A34 (2012)
- [25] D. Babich, Phys. Rev. D **72**, 066902 (2005)
- [26] P. Cabella, et al., Mon. Not. Roy. Astron. Soc. **405**, 961 (2010)
- [27] B. Casaponsa, R.B. Barreiro, A. Curto, E. Martínez-González, P. Vielva, Mon. Not. Roy. Astron. Soc. **411**, 3, 2019 (2011)
- [28] B. Casaponsa, et al., Mon. Not. Roy. Astron. Soc. **416**, 457 (2011)
- [29] A. Curto, et al., Mon. Not. Roy. Astron. Soc. **393**, 615 (2009)
- [30] S. Donzelli, F.K. Hansen, M. Liguori, D. Marinucci, S. Matarrese, Astrophys. J. **755**, 19 (2012)
- [31] A. Ducout, F. Bouchet, S. Colombi, D. Pogosyan, S. Prunet, arXiv:1209.1223
- [32] J.R. Fergusson, M. Liguori, E.P.S. Shellard, JCAP **12**, 032 (2012)
- [33] T. Matsubara, Phys. Rev. D **81**, 083505 (2010)
- [34] H.U. Nørgaard-Nielsen, Astron. Astrophys. **520**, A87

- (2010)
- [35] F. Noviello, *New Astron.* **14**, 659 (2009)
- [36] G. Rossi, P. Chingangbam, C. Park, *Mon. Not. Roy. Astron. Soc.* **411**, 1880 (2011)
- [37] D. Pietrobon, P. Cabella, A. Balbi, G.D. Gasperis, N. Vittorio, *Mon. Not. Roy. Astron. Soc.* **396**, 1682 (2009)
- [38] D. Pietrobon, A. Balbi, P. Cabella, K.M. Górski, *Astrophys. J.* **723**, 1 (2010)
- [39] G. Pratten, D. Munshi, *Mon. Not. Roy. Astron. Soc.* **423**, 3209 (2012)
- [40] T.L. Smith, M. Kamionkowski, B.D. Wandelt, *Phys. Rev. D* **84**, 063013 (2011)
- [41] P. Vielva, J.L. Sanz, *Mon. Not. Roy. Astron. Soc.* **397**, 837 (2009)
- [42] A.P.S. Yadav, et al., *Astrophys. J.* **678**, 578 (2008)
- [43] W. Zhao, *Mon. Not. Roy. Astron. Soc.* (2013). doi:10.1093/mnras/stt979
- [44] E. Komatsu, et al., *Astrophys. J. Suppl.* **148**, 119 (2003)
- [45] A.P.S. Yadav, B.D. Wandelt, *Adv. Astron.* 565248 (2010)
- [46] L.-Y. Chiang, P.D. Naselsky, P. Coles, *Astrophys. J.* **664**, 8 (2007)
- [47] L.R. Abramo, T.S. Pereira, *Adv. Astron.* 378203 (2010)
- [48] N. Bartolo, S. Matarrese, A. Riotto, *Adv. Astron.* **157079** (2010)
- [49] A. Bernui, C. Tsallis, T. Villela, *Phys. Lett. A* **356**, 426 (2006); *Europhys. Lett.* **78**, 19001 (2007)
- [50] M. Cruz, E. Martínez-González, P. Vielva, arXiv:0901.1986
- [51] E. Komatsu, *New Astron. Rev.* **47**, 8-10, 797 (2003)
- [52] B. Lew, *JCAP* **08**, 017 (2008)
- [53] J.D. McEwen, M.P. Hobson, A.N. Lasenby, D.J. Mortlock, *Mon. Not. Roy. Astron. Soc.* **388**, 659 (2008)
- [54] C.G. Park, *Mon. Not. Roy. Astron. Soc.* **349**, 313 (2004)
- [55] G. Rossmanith, C. Räth, A.J. Banday, G. Morfill, *Mon. Not. Roy. Astron. Soc.* **399**, 1921 (2009)
- [56] C. Räth, G. Rossmanith, G. Morfill, A.J. Banday, K.M. Górski, arXiv:1005.2481
- [57] C. Räth, et al., *Mon. Not. Roy. Astron. Soc.* **415**, 2205 (2011)
- [58] Y. Wiaux, P. Vielva, R.B. Barreiro, E. Martínez-González, P. Vanderghenst, *Mon. Not. Roy. Astron. Soc.* **385**, 939 (2008)
- [59] P. Bielewicz, H.K. Eriksen, A.J. Banday, K.M. Górski, P.B. Lilje, *Astrophys. J.* **635**, 750 (2005)
- [60] P. Bielewicz, B.D. Wandelt, A.J. Banday, arXiv:1207.6905
- [61] C.J. Copi, D. Huterer, D.J. Schwarz, G.D. Starkman, *Adv. Astron.* 847541 (2010)
- [62] M. Cruz, L. Cayon, E. Martínez-González, P. Vielva, J. Jin, *Astrophys. J.* **655**, 11 (2007)
- [63] A. Gruppuso, K.M. Górski, *JCAP* **03**, 019 (2010)
- [64] A. Gruppuso, et al., *Mon. Not. Roy. Astron. Soc.* **411**, 1445 (2011)
- [65] P. Vielva, E. Martínez-González, E.B. Barreiro, J.L. Sanz, L. Canyon, *Astrophys. J.* **609**, 22 (2004)
- [66] P. Vielva, Y. Wiaux, E. Martínez-González, P. Vanderghenst, *Mon. Not. Roy. Astron. Soc.* **381**, 932 (2007)
- [67] A. Bernui, M.J. Rebouças, *Phys. Rev. D* **79**, 063528 (2009)
- [68] A. Bernui, M.J. Rebouças, *Phys. Rev. D* **81**, 063533 (2010)
- [69] A. Bernui, M.J. Rebouças, *Phys. Rev. D* **85**, 023522 (2012)
- [70] J.M. Bardeen, *Phys. Rev. D* **22**, 1882 (1980); J.M. Bardeen, et al., *Astrophys. J.* **304**, 15 (1986)
- [71] H. Kodama, M. Sasaki, *Prog. Theor. Phys. Suppl.* **78**, 1 (1984)
- [72] R.K. Sachs, A.M. Wolfe, *Astrophys. J.* **147**, 73 (1967);
- [73] F. Elsner, B.D. Wandelt, *Astrophys. J. Suppl.* **184**, 264 (2009)
- [74] A. Bernui, M.J. Rebouças, A.F.F. Teixeira, *Int. J. Mod. Phys.: Conf. Ser.* **03**, 286 (2011)
- [75] K.M. Górski, et al., *Astrophys. J.* **622**, 759 (2005)
- [76] Planck Collaboration: P.A.R. Ade, et al., arXiv:1303.5084
- [77] W.A. Cardona, A. Bernui, M.J. Rebouças, *Int. J. Mod. Phys. Conf. Ser.* **18**, 286 (2012)